A Synthesized Global Neutron Map

Anthony L Hutcheson
Space Science Division
U.S. Naval Research Laboratory
Washington, DC, USA
anthony.hutcheson@nrl.navy.mil
https://orcid.org/0000-0002-0283-9163

Bernard F. Phlips
Space Science Division
U.S. Naval Research Laboratory
Washington, DC, USA
bernard.phlips@nrl.navy.mil

Lee J. Mitchell
Space Science Division
U.S. Naval Research Laboratory
Washington, DC, USA
lee.mitchell@nrl.navy.mil

Byron E. Leas
General Dynamics Information Technology, Inc.
Falls Church, VA, USA
byron.leas.ctr@nrl.navy.mil

***Abstract*— We have synthesized a global neutron map showing relative neutron fluxes at locations all over the world based on the effects of elevation, geomagnetic rigidity, solar cycle, and the presence of ground moisture and/or bodies of water. The modeled values show good agreement with measured data, indicating that the considered factors represent the largest effects on local neutron flux. This synthesized map helps address one of the challenges of reliably sensing potential nuclear threats – the variability of the natural neutron background with location and time.**

Keywords—cosmic rays, background radiation, cosmogenic neutrons

I. Introduction

Sensing characteristic ionizing radiation --- i.e., gamma rays and neutrons – is well recognized as one of the primary means of detecting potential nuclear threats that could be transported into and within the United States. For example, the Security and Accountability for Every Port Act of 2006 (or the Safe Port Act, H.R. 4954) required that "all containers entering high volume U.S. ports by vessel to be scanned for radiation" and that the Secretary of Homeland Security "develop a strategy for the deployment of radiation detection capabilities". By and large, the radiation detection capabilities that have been deployed consist of large-scale radiation systems known as radiation portal monitors (RPMs) or handheld radiation detection systems used for secondary (or more localized) screening. These systems generally comprise ^{3}He gas proportional detectors to sense neutrons emitted by certain nuclear materials and/or scintillator sensors (e.g., polyvinyltoluene or sodium iodide) to detect emitted gamma rays. As ^{3}He detectors do not provide spectroscopic information, neutron detection is determined solely by comparing gross detector count rates to the expected background neutron detection rate at that location.

One of the challenges in sensing potential nuclear threats is successfully detecting and identifying the inherently low signal emitted by these objects. For example, the neutron flux from 1 kg of weapons-grade plutonium (WGPu) at a distance of 10 m is on the order of 10^{-3} neutrons/cm^2/s; for the same mass of weapons-grade uranium (WGU), the neutron flux is closer to 10^{-7} neutron/cm^2/s [1]. For comparison, the background neutron rate at sea level in the energy range of interest for fission-spectrum neutrons (100 keV to 10 MeV) is on the order of 10^{-3} neutrons/cm^2/s [2], similar to that of the WGPu and much larger than that of the WGU. In addition, the radiation background varies based on location, weather, and other external factors. In order to successfully define a detection threshold that allows for the maximum sensitivity while maintaining a low level of false positive (nuisance) alarms, one must have good knowledge of the natural radiation background.

Toward this end, the U.S. Naval Research Laboratory (NRL) has synthesized a global neutron background map using publicly available datasets. This map incorporates the largest known effects on local neutron background – elevation, geomagnetic rigidity, solar cycle, and ground moisture/bodies of water – and attempts to create an accurate representation of the natural neutron background at locations all over the world.

II. Global Neutron Map

The natural neutron background measured a given location is almost entirely cosmogenic in origin; cosmic rays interact with the atmosphere to produce neutrons ranging in energy from meV to GeV. The flux of these neutrons at a given point on the Earth's surface is dependent on many factors, including the geomagnetic rigidity and solar cycle (which affect the quantity and energy of cosmic rays that reach the Earth's atmosphere), the amount of atmosphere through which the neutrons must propagate, and the surrounding moderators at the location at which the measurement is being performed. We seek to utilize the current understanding of how each of these parameters affects the neutron flux along with publicly available datasets to create an accurate map of the global neutron background.

The global neutron map provides a neutron flux scaling factor for each location on the map. This scaling factor is normalized to a value of one for New York City at sea level and "mid-level" solar activity (defined as a monthly average sunspot number of 82.5). For a given neutron detector configuration, if the measured background flux for Condition 1 is φ_1, the expected measured background flux for Condition 2 can be found by using the scaling factor F for each condition:

$$\varphi_2 = \varphi_1 \cdot \left(\frac{F_2}{F_1}\right) \quad (1)$$

This work was supported by the Chief of Naval Research.

These changes in condition can be spatial or temporal; the global neutron map can be used to predict the expected measured background for two different locations during the same general time, for two different times at the same location, or for two completely different locations and times.

The following sections detail the implementation of each of the major effects on the local neutron background into the global neutron map before demonstrating the combined product and comparing to measured data.

A. Elevation

Elevation affects the neutron flux primarily via exponential attenuation; as elevation increases, there is less grammage of air to attenuate the cosmogenic neutrons (see Fig. 1). This attenuation as a function of the atmospheric depth d is captured by the following scaling factor [2]:

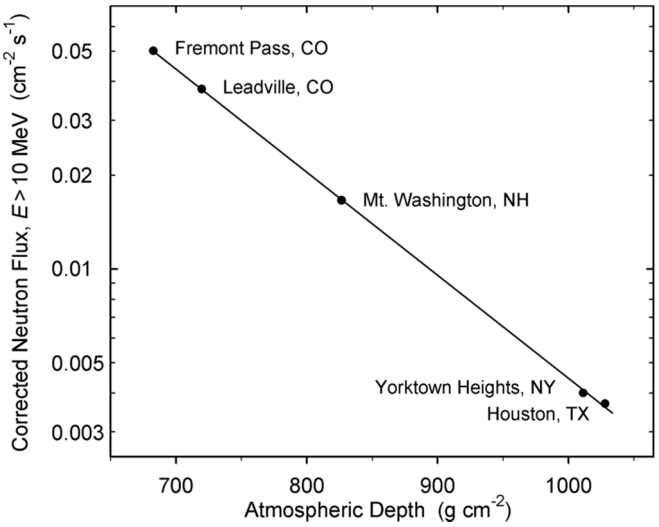

Fig. 1. Neutron flux above 10 MeV at five measurement locations as a function of atmospheric depth (points) [2].

$$F_{alt}(d) = \exp\left[\frac{d_{SL}-d}{L_n}\right] \quad (2)$$

where $d_{SL} = 1033.7$ g/cm^2 is the atmospheric depth at sea level and $L_n = 131.3$ g/cm^2 is the effective attenuation length in the atmosphere for neutrons above 10 MeV.

There are many elevation datasets available in various formats and using various methods. However, there are not many datasets available that map the entire globe. For the purposes of this application, two elevation datasets were utilized: Worldwind [3] and Panoramas [4].

B. Geomagnetic Rigidity and Solar Cycle

Neutron background fluctuates as an interconnected function of geomagnetic rigidity cutoff and solar activity. Geomagnetic rigidity cutoff is a measure of the shielding effect of the Earth's magnetosphere as a function of latitude and longitude; it gives the minimum magnetic rigidity of an incoming particle to penetrate the geomagnetic field. Solar activity refers to the nearly periodic cycle of changes in solar radiation and the ejection of solar material by the Sun; this cycle spans approximately eleven years.

Generally, the effects of these two phenomena are described by depth-dependent Dorman functions parametrized by Belov, Struminsky, and Yanke and defined at solar minimum and solar maximum [5]; for solar activity between the two extremes, the function is simply interpolated between the two known values. However, although solar activity at solar minimum is well defined (a monthly averaged sunspot number of zero), "solar maximum" can vary from cycle to cycle (see Fig. 2). Therefore, for this work, an adjusted Belov, Struminsky, and Yanke factor was determined. The effects of geomagnetic rigidity cutoff and solar activity on the local neutron background for a given latitude and longitude are then given by the following scale factor:

$$F_{RigSol}(R, d, S) = F_{BSY_{min}}(R, h(d)) \cdot (1 + \beta(R) \cdot S) \quad (3)$$

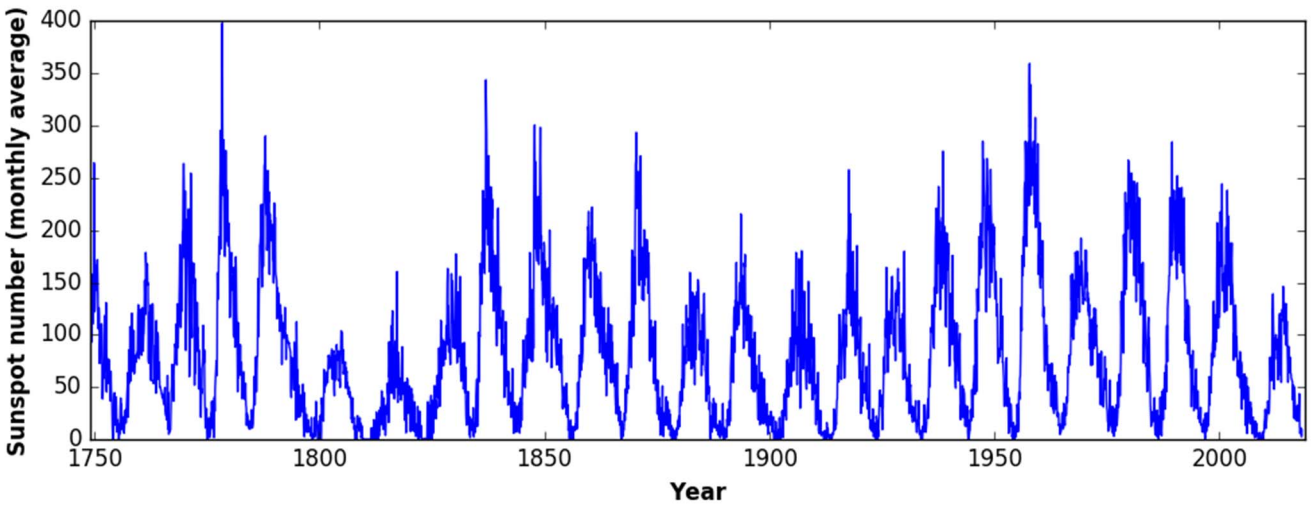

Fig. 2. Monthly averaged sunspot number as a function of time [6].

978-1-7281-5092-5/19/$31.00 ©2019 IEEE

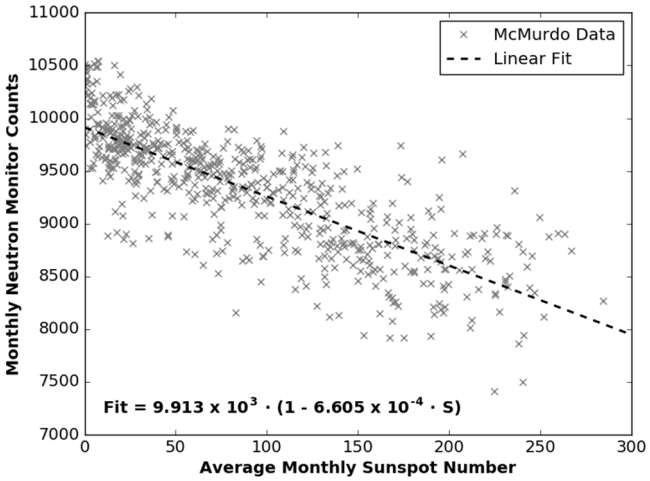

Fig. 3. The reported monthly average neutron monitor counts in McMurdo, Antarctica, as a function of average monthly sunspot number. The cutoff rigidity at this location is approximately 0.01 GV.

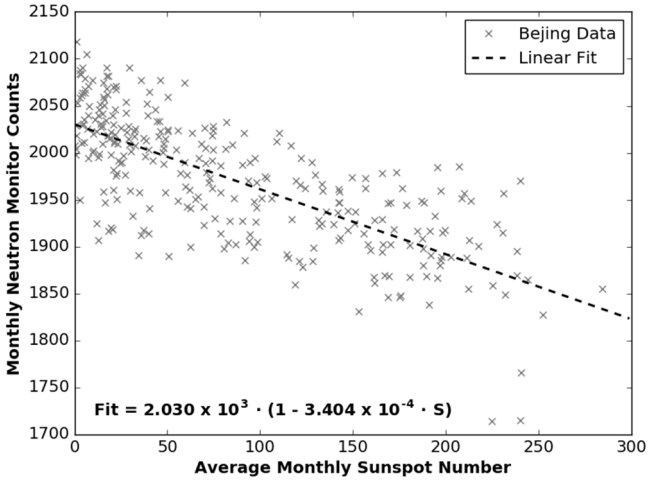

Fig. 4. The reported monthly average neutron monitor counts in Bejing, China, as a function of average monthly sunspot number. The cutoff rigidity at this location is approximately 9.56 GV.

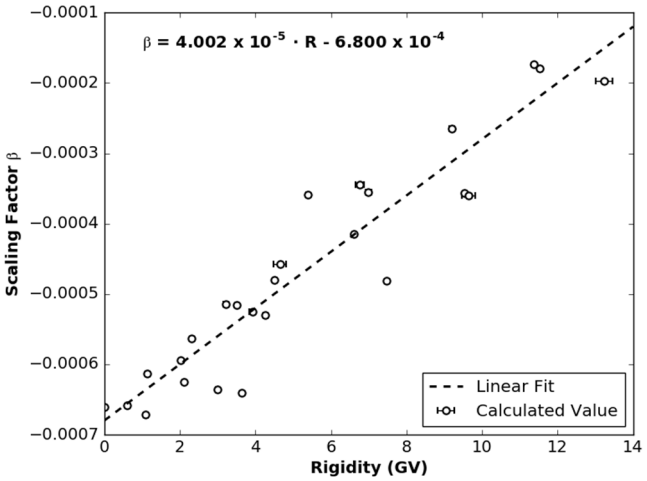

Fig. 5. The calculated scaling factor β as a function of cutoff rigidity for 26 different neutron monitor stations around the world. The linear fit to these values is used as the functional form of β(R) for the global neutron map.

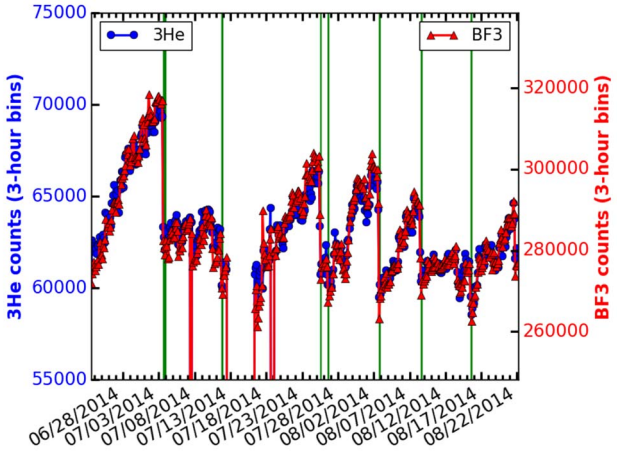

Fig. 6. Measured neutron counts near Starke, FL, as a function of time. Periods of greater than 0.5" of rainfall are highlighted in green [8].

where $F_{BSY_{min}}$ is the Belov, Struminsky, and Yanke factor at solar minimum, R is the cutoff rigidity in units of GV at a given latitude and longitude, $h(d)$ is the barometric pressure in units of bar at an atmospheric depth d, S is the monthly averaged international sunspot number, and β is a scaling factor determined by fitting recorded neutrons counts from multiple global neutron monitors with various cutoff rigidities as a function of sunspot number.

To determine the functional form of $\beta(R)$, the monthly neutron monitor counts C_N for 26 different neutron monitor stations around the world were plotted against the monthly average sunspot number S. The neutron monitor counts were taken from the Neutron Monitor Database (NMDB) [7], which distributes official data provided by neutron monitor stations. The plotted data were fit to a linear function of the form $C_N = C_0 \cdot (1 + \beta \cdot S)$, where C_0 is the expected monthly neutron monitor counts at solar minimum. Figs. 3 and 4 demonstrate this process for neutron monitor stations in McMurdo, Antarctica, and Bejing, China, yielding β values of -6.605 × 10^{-4} and -3.404 × 10^{-4}, respectively. The values of β for all 26 stations were then plotted as a function of the reported cutoff rigidity R at each station, and the plotted data were fit to a linear function to yield a functional form of $\beta(R)$. Fig. 5 shows the plotted data and associated fit, with a functional form of

$$\beta(R) = 4.002 \times 10^{-5} \cdot R - 6.800 \times 10^{-4} \qquad (4)$$

C. *Ground Moisture and Bodies of Water*

Significant quantities of hydrogenous materials have the effect of reducing local neutron background due to downscatter and capture mechanisms. In most cases, the dominant sources of local hydrogenous materials are soil moisture and/or local bodies of water. For example, Fig. 6 demonstrates the effect on the measured background neutron count rate as a function of time in Starke, FL. After a significant rainfall, the ground

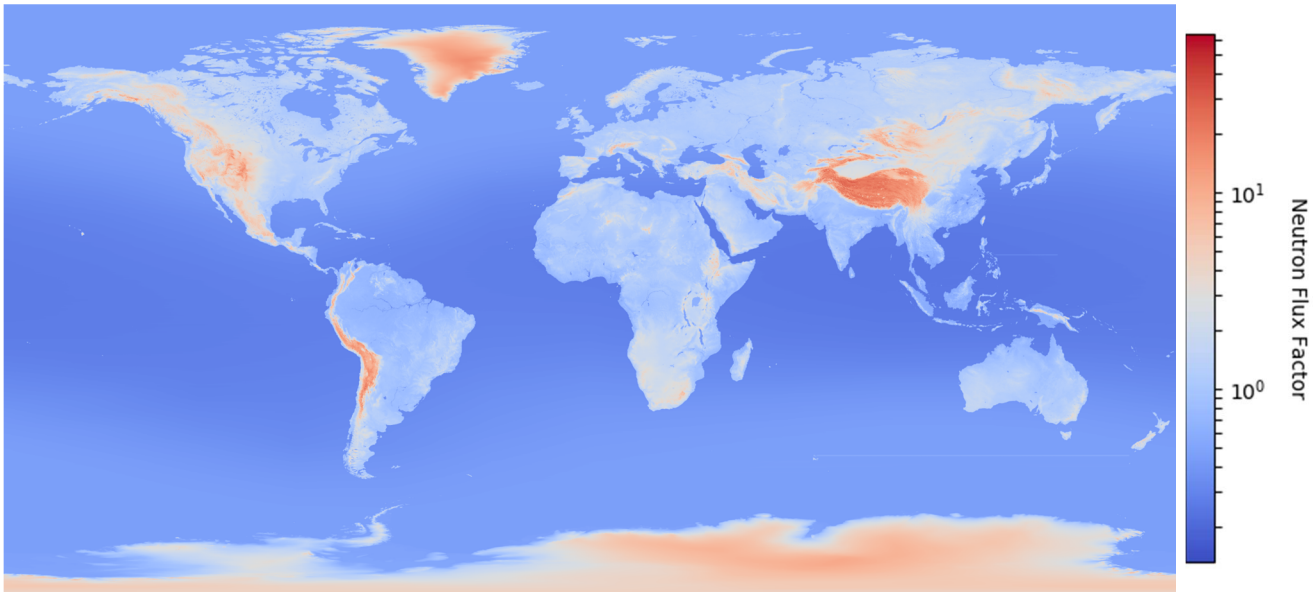

Fig. 7. Synthesized global map of the neutron flux scaling factor. This map has ~25,000,000 flux values at a resolution of 5.56 km

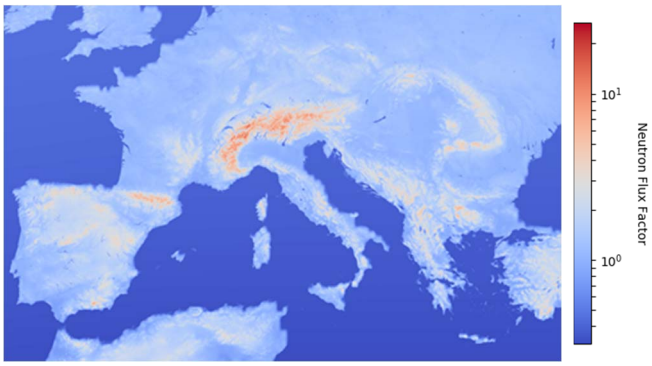

Fig. 8. Synthesized map of the neutron flux scaling factor for southern Europe. Spatial resolution is 90 m.

moisture level is increased, and the measured neutron count rate is greatly reduced. Between rainfall events, drainage and evaporation slowly reduce the ground moisture, and the measured neutron count rates slowly increase. The effect of local soil moisture and/or bodies of water on the neutron background was determined by Desilets et al. [9] by fitting ground-level neutron fluxes from Monte Carlo simulations and is given by the following scale factor:

$$F_{mois}(\vartheta) = \frac{0.0808}{\vartheta + 0.115} + 0.372 \quad [\vartheta \geq 0.02] \tag{5}$$

where ϑ is the average volumetric soil moisture content (in units of kg/kg) for a given latitude and longitude. For open water areas, $\vartheta = 1$. As the expression in (1) is only valid for values of $\vartheta \geq 0.02$ kg/kg, for soil moisture contents below that threshold, we used a simple linear extrapolation to an assumed value of $F_{mois}(0) = 1$:

$$F_{mois}(\vartheta) = -1.4741 \cdot \vartheta + 1.0 \quad [\vartheta < 0.02] \tag{6}$$

To provide a proper scaling to New York City at sea level, the factor as applied in this program is:

$$F_{adj\_mois} = \frac{F_{mois}(lat,lon)}{F_{mois}(NYC)} \tag{7}$$

Ground moisture values were taken from the Global Land Data Assimilation System (GLDAS) Noah model [10]. Currently, the soil moisture value for a given location during a given month is taken to be the average soil moisture for that month as modeled for the year 2017.

D. Combined Effects

The combined neutron flux scaling factor is taken to be the product of each of the individual scaling factors:

$$F(d,R,S,\vartheta) = F_{alt}(d) \cdot F_{RigSol}(R,d,S) \cdot F_{adj\_mois}(\vartheta) \tag{8}$$

The global synthesized map of this neutron flux scaling factor is shown in Fig. 7. This map represents approximately 25,000,000 scaling factor values and has a resolution of 5.56 km. The resolution of this map is primarily dictated by computer run time; the map shown in Fig. 7 took 4 hours to produce on a standard laptop. A representative map of the neutron flux scaling factor at higher resolution is shown for southern Europe in Fig. 8; the spatial resolution of this map is 90 m and is dictated primarily by the resolution of the datasets used to synthesize the map.

There are local factors that may be expected to affect neutron flux that are not considered in the current global neutron model, including weather-related pressure changes, overhead grammage in "urban canyons", local foliage density, and instantaneous ground moisture changes due to rainfall/drainage/evaporation. For most of these factors, the effect is expected to be comparatively small. For example, weather variation in atmospheric pressure is usually less than a

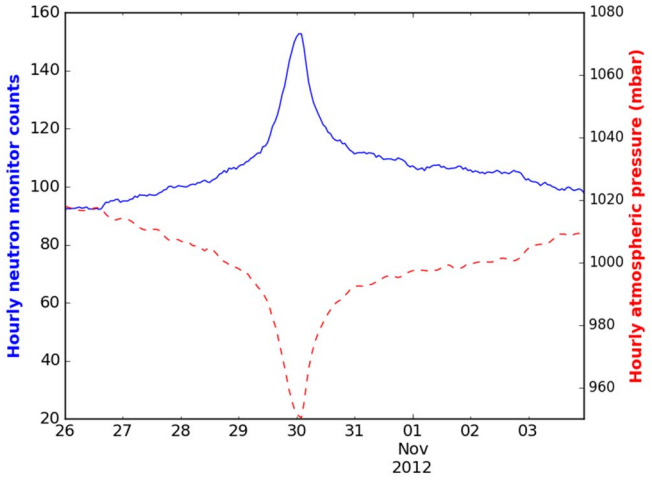

Fig. 9. Hourly neutron monitor counts (solid blue line) and reported atmospheric pressure (dashed red line) as a function of time during Hurricane Sandy [7].

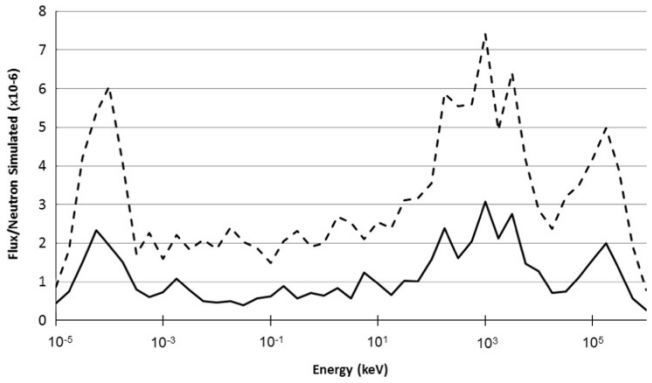

Fig. 10.Simulated neutron background spectrum for downtown Chicago (solid line) as well as for a "reduced height" Chicago model (dashed line) [14].

percent -- for the first two weeks of July 2019, the standard deviation in the mean atmospheric pressure at Ronald Reagan Washington National Airport in Arlington, VA, was 0.3% [11], which is equivalent to a neutron flux standard deviation of approximately 2.3%. (It should be noted, however, that extreme weather events can lead to significant changes in the neutron background rate; for example, during Hurricane Sandy in 2012, the neutron count rate at the neutron monitor station in Newark, NJ, rose by over 50% [12]; see Fig. 9.) Other factors, such as instantaneous ground moisture changes due to rainfall or the overhead shielding in urban areas, may have a sizable effect (see the ~20% change in neutron count rate shown in Fig. 6 or the factor of 2-3 difference in Fig. 10) but lack a feasible way to incorporate into the predictive neutron model.

E. Comparison to Measured Data

The modeled neutron flux scaling factor was compared to neutron background measurements collected using an unmoderated Radpack-GC ^{3}He detector [13] at various locations and times [14, 15]. Comparisons to data measured in three regions (Sandia Peak in Albuquerque, NM; Mauna Kea/Mauna Loa on the island of Hawai'i; and the DC-VA-MD metro area) are shown in Fig. 11, demonstrating good agreement between the modeled and measured values.

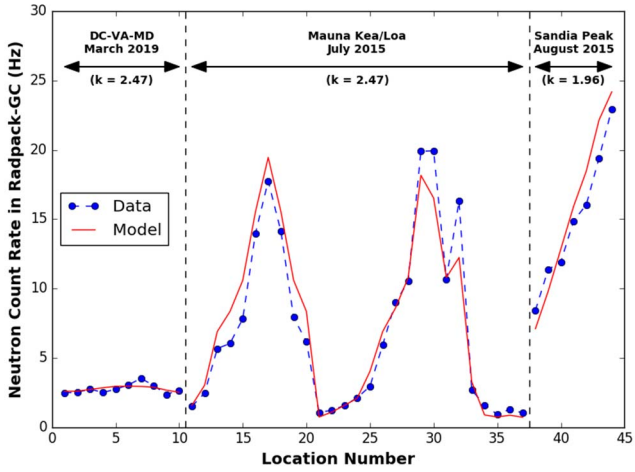

Fig. 11. Comparison of the measured neutron rate in an unmoderated Radpack-GC ^{3}He detector (blue circles) to the (scaled) modeled values from the synthesized global neutron map.

III. Conclusion

We have synthesized a global neutron map showing relative neutron fluxes based on the effects of elevation, geomagnetic rigidity, solar cycle, and the presence of ground moisture and/or bodies of water. The modeled values show good agreement with measured data, indicating that the considered factors represent the largest effects on local neutron flux. Better agreement to measured data may be achieved by using datasets with finer spatial resolution and with more accurate knowledge of the instantaneous ground moisture levels for each location. In addition, the inclusion of other factors (e.g., snow/ice cover, soil composition, urban shielding from buildings, vegetation) may further improve the modeled values and should be considered for future work.

References

[1] S. Fetter et al., "Detecting nuclear warheads," Science and Global Security, vol. 1, pp. 225-302, 1990,

[2] M.S. Gordon et al., "Measurement of the flux and energy spectrum of cosmic-ray induced neutrons on the ground," in IEEE Transactions on Nuclear Science, vol. 51, no. 6, pp. 3427–3434, Dec. 2004.

[3] [Online]. Available: http://cloudcapsupport.com/elevation/. [Accessed: June 2018].

[4] J. deFerranti, "Digital Elevation Data", [Online]. Available: http://viewfinderpanoramas.org/dem3.html. [Accessed: June 2018].

[5] A. Belov, A. Struminsky, and V. Yanke, "Neutron monitor response functions for galactic and solar cosmic rays," in ISSI Workshop on Cosmic Rays and Earth, 1999.

[6] SILSO, World Data Center – Sunspot Number and Long-term Solar Observations, Royal Observatory of Belgium, [Online]. Available: http://www.sidc.be/SILSO/. [Accessed: May 2018].

[7] Neutron Monitor Database. [Online]. Available: http://www.nmdb.eu. [Accessed: May 2018]

[8] A.L. Hutcheson et al., “Effects of rain and soil moisture on background neutron measurements with the SuperMISTI neutron array,” Radiation Measurements, vol. 99, pp. 50-59, Apr. 2017.

[9] D. Desilets, M. Zreda, and T.P.A Ferré, “Nature’s neutron probe: land surface hydrology at an elusive scale with cosmic rays,” Water Resources Research, vol. 46, no. 11, Nov. 2010.

[10] M. Rodell et al., “The global land data assimilation system,” Bulletin of the American Meteorological Society, vol. 85, no. 3, pp. 381-394, Mar. 2004.

[11] [Online]. Available: https://www.wunderground.com. [Accessed: August 2019].

[12] P. Goldhagen, “Use of cosmic-ray neutron data in nuclear threat detection and other applications,” Neutron Monitor Community Workshop, Honolulu, HI, 2015.

[13] Sensor Technology Engineering, Inc. [Online]. Available: http://www.radiationpager.com. [Accessed: November 2017].

[14] L.J. Mitchell et al., “Gamma-ray and neutron background comparison of US metropolitan areas,” Nuclear Instruments and Methods in Physics Research Section A: Accelerators, Spectrometers, Detectors and Associated Equipment, vol. 784, pp. 311-318, Jun. 2015.

[15] R.S. Woolf et al., “Measurement of secondary cosmic-ray neutrons near the geomagnetic North Pole,” Journal of Environmental Radioactivity, vol. 198, pp. 189-199, Mar. 2019.

978-1-7281-5092-5/19/$31.00 ©2019 IEEE